Heliyon 9 (2023) e16276

Contents lists available at ScienceDirect

Heliyon

journal homepage: www.cell.com/heliyon

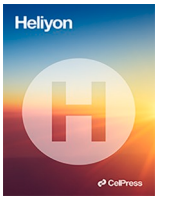

Research article

Investigation on the physical and electrochemical properties of typical Ni-based alloys used for the bipolar plates of proton exchange membrane fuel cells

Jiacheng Zhong [a], Beirui Hou [a], Wenmin Zhang [a], Zhansheng Guo [b], Chunwang Zhao [a,c,*]

[a] School of Materials Science and Hydrogen Energy, Foshan University, Foshan 528000, China
[b] School of Mechanics and Engineering Science, Shanghai University, Shanghai 200072, China
[c] Guangdong Key Laboratory for Hydrogen Energy Technologies, Foshan, 528000, China

ARTICLE INFO

Keywords:
Corrosion resistance
Hydrophobicity
Interfacial contact resistance
Hardness
Tensile strength

ABSTRACT

The phase, mechanical properties, corrosion resistance, hydrophobicity, and interface contact resistance of three typical Ni-based alloys (Hastelloy B, Hastelloy C-276, and Monel 400) and 304 stainless steels were experimentally studied to evaluate their service performances as bipolar plate materials of proton exchange membrane fuel cells. All four alloys exhibit single-phase face-centered cubic structure, high strength, good ductility, and high hardness. Hastelloy C-276 has the best ductility with an uniform elongation of 72.5% and highest hardness of 363.7 HV. Hastelloy B has the highest ultimate tensile strength of 913.6 MPa. The hydrophobicity of all four alloys is not good, although Monel 400 has the highest water contact angle of 84.2°. Hastelloy B, Hastelloy C-276, and 304 stainless steel exhibit unsatisfying corrosion resistance in a simulated acidic work environment of proton exchange membrane fuel cell (0.5 M H_2SO_4+2 ppm HF, 80 °C, H_2) and high interface contact resistance. By contrast, Monel 400 demonstrates excellent corrosion resistance with a corrosion current density of 5.9×10^{-7} A cm^{-2} and a low interface contact resistance of 7.2 mΩ cm^2 at 140 N/cm^2. In terms of comprehensive performance, Monel 400 is the best uncoated material for the bipolar plates of proton exchange membrane fuel cells among typical Ni-based alloys.

1. Introduction

Owing to the overuse of fossil fuels, the global climate has changed considerably. Achieving carbon neutrality is an irreversible trend because of the increasing demand for environmental protection [1,2]. Proton exchange membrane fuel cells (PEMFCs) have great potential for energy transformation as a clear energy technology in several areas, such as transportation, because they can use hydrogen as fuel [3]. Bipolar plates are the main component of a PEMFC and undertake the key roles of supporting the membrane electrode assembly and collecting the current. Although graphite has good chemical stability and conductivity, its poor mechanical properties hinder its wide commercial application, such as in cars. Metal bipolar plates have become a highly desired candidate due to their good mechanical properties and good conductivity. However, metals are prone to corrosion when exposed to the acidic work

* Corresponding author. School of Materials Science and Hydrogen Energy, Foshan University, Foshan 528000, China.
E-mail address: zhaocw@fosu.edu.cn (C. Zhao).

https://doi.org/10.1016/j.heliyon.2023.e16276
Received 13 January 2023; Received in revised form 5 May 2023; Accepted 11 May 2023
Available online 15 May 2023

Table 1
Elemental composition of the four alloys (wt. %).

Alloys	Ni	Cr	Fe	Mo	Mn	Si	Cu	Others
Hastelloy B	78.0	0.5	1.1	20.1	0.3	/	/	/
Hastelloy C-276	60.3	19.7	6.4	11.6	0.5	/	/	W 1.5
Monel 400	63.9	/	2.1	/	1.7	1.8	30.1	S 0.4
304SS	7.2	20.9	69.9	/	1.0	0.9	/	C 0.1

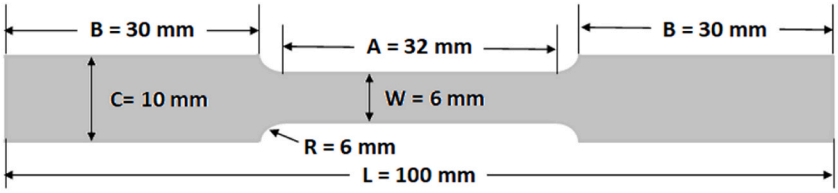

Fig. 1. Geometry of tensile samples.

environments of PEMFC, and the corrosion products can reduce the output performance of PEMFC. To adapt to this acidic work environment and improve the conductivity, many researchers tried to cover conductively coatings on the surface of metal bipolar plate [4,5]. However, current coating preparation technologies, such as physical vapor deposition [6] and chemical vapor deposition [7], require a complex and time-consuming process, resulting in high costs and great difficulty in practical application. Selecting appropriate metal bipolar plate materials for PEMFC application from existing corrosion resistance materials may be another effective and practical route.

Stainless steels and Ni-based alloys are two kinds of widely used corrosion resistant materials [8]. Stainless steels have good mechanical properties and low price and thus received the most research interest for PEMFC bipolar plate application. Unfortunately, the corrosion resistance and conductivity of stainless steels cannot meet the 2025 US. Department of Energy (DOE) targets for bipolar plate [9] and thus are not good enough under the acidic work environments of PEMFCs. As another excellent corrosion resistant material, Ni-based alloys have been frequently used in chemical, petroleum, aerospace, and other industries [10]. Among them, Hastelloy alloys and Monel alloys are typical commercial Ni-based alloys. Owing to its high Cr and Mo contents, Hastelloy C-276 is able to withstand oxidizing acids, such as H_2SO_4. Li et al. [11] investigated the oxidation behavior of Hastelloy C-276 in two harsh environments: high temperature air and supercritical water. They found that corrosion rates in supercritical water vaporization environments were 2.5–3 times higher than in high-temperature air. In addition, the presence of element W in Hastelloy C-276 leads to grain refinement [12], which provides good corrosion resistance and mechanical properties [13]. Hastelloy B has relatively high Mo contents and thus has good corrosion resistance against medium concentrations of sulfuric acid solutions (or contains a certain amount of chloride ions) [14]. Ni–Cu alloys, such as Monel alloys, have received increasing attention from researchers because of their excellent corrosion resistance [15]. Kannan et al. [16] used wire arc additive manufacturing (WAAM) to deposit Monel FM60 single-pass multilayer walls on Inconel 625 substrates. The results showed that the corrosion rate of the prepared coating was low because WAAM is effective in maintaining the passivation behavior of the Ni–Cu alloy.

Although Hastelloy B, Hastelloy C-276, and Monel 400 have been applied in various harsh corrosion environments and have shown good corrosion resistance, their service performances in PEMFC environment as uncoated bipolar plate materials remain unclear. In this work, the phase, mechanical properties, corrosion resistance, hydrophobicity, and interface contact resistance (ICR) of these three typical Ni-based alloys were comprehensively studied. For comparison, 304 stainless steel (304SS) was also evaluated.

2. Experimental methods

2.1. Preparation of samples

Commercially available Hastelloy B, Hastelloy C-276, Monel 400, and 304SS were used in this work. Table 1 shows the elemental composition of the four alloys measured by energy dispersion spectroscopy. The tensile testing samples were cut into dog bone shapes (Fig. 1) using wire cut electrical discharge machining in accordance with ASTM E8/E8M−22 Standard Test Methods for Tension Testing of Metallic Materials. The cut surfaces of the samples were grinded with SiC paper and then polished with emery cloth. The samples for hydrophobicity test were plates with dimensions of 20 mm × 20 mm × 2 mm. The samples for electrochemical property test were disc with a diameter of 15 mm and a thickness of 2 mm. The samples for ICR test were plates with dimensions of 50 mm × 50 mm × 2 mm.

2.2. Characterization

The phase of the four alloys was examined by a Tongda TD-3500 X-ray diffractometer (XRD) using a Cu Kα source of radiation (λ = 0.15406 nm). The surface morphology and composition of the four alloys were examined using a Hitachi SU-1500 scanning electron

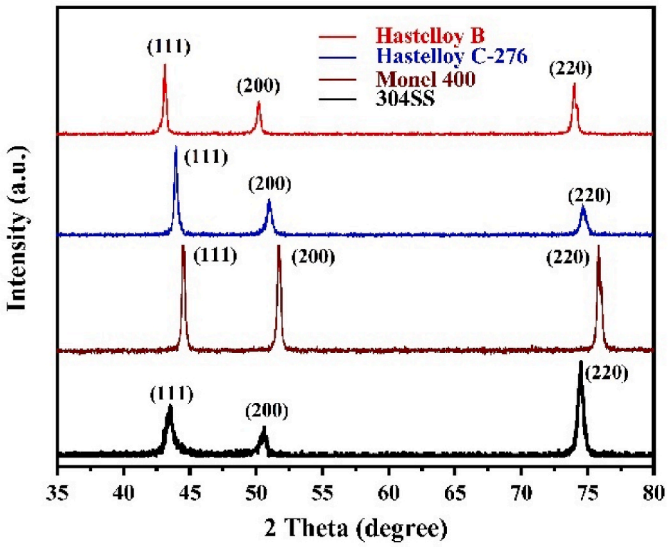

Fig. 2. XRD patterns of the four alloys.

microscope (SEM) equipped with a Horiba EMAX x-act X-ray energy dispersion spectrometer at an accelerating voltage of 20 kV and a beam current of 100 μA.

2.3. Hydrophobicity test

Water contact angle (WCA) was measured using a video-based optical instrument (JC2000D1B) with 5 μL of deionized water droplets. Contact angle values were represented by the average of 10 measurements for each alloy to minimize errors. A Bruker Dimension Icon atomic force microscope (AFM) operating in a tapping mode was used to capture the images of the alloy surfaces. The nanoprobe cantilever was made of silicon nitride (Si_3N_4) with a spring constant of k = 40 N/m. The scanning area was 4 μm × 4 μm, and three areas were selected for each alloy. The surface roughness of each alloy was measured using NanoScope Analysis software.

2.4. Mechanical property test

Uniaxial tensile tests were conducted using an MTS Landmark testing machine with a tensile rate of 1 mm/min. During the test, displacement measurements were performed using a video extensometer (gauge length 25 mm). Three tensile testing samples of each alloy were prepared and tested. Vickers hardness tests were conducted using a HXS-1000tac microhardness tester with a load of 200 N and a holding time of 15 s following the ASTM E384-22 Standard Test Method for Microindentation Hardness of Materials. Before testing, the microhardness tester was calibrated using a standard hardness block ($238HV_{0.2}$). Ten indentations were carried out for each alloy to minimize the measuring error.

2.5. Electrochemical property test

Electrochemical properties tests were performed in a three-electrode system (platinum sheet as the counter electrode, saturated calomel electrode (SCE) as the reference electrode, and sample as the working electrode), in which 1 cm^2 of the sample surface area was exposed to the electrolyte using a CorrTest CS150 M electrochemical workstation. The electrolyte was made of 0.5 M H_2SO_4+2 ppm HF, which is similar to the acidic work environments of PEMFC [17]. The samples were first immersed into the electrolyte for 1 h while the open circuit potential tests were performed. Potentiodynamic polarization test was performed in the range of −0.6 V to +1.2 V at a scanning speed of 0.2 mV/s. Corrosion potentials and corrosion current densities were obtained by Tafel extrapolation implemented in the electrochemical analysis software. Tafel fitting was performed in the potential range of ±200 mV around the open circuit potential. Electrochemical properties tests were conducted at 80 °C with H_2 bubble at a gas flow rate of 20 mL/min. All samples were weighed five times using an analytical balance before and after the electrochemical property test.

2.6. Interfacial contact resistance (ICR) test

ICR was measured as previously described [18]. The test setup was composed of three parts: 1. a Testometric M350-CT universal tester was used for providing compaction force and recording data, 2. copper electrode with Au coating and carbon paper were used to simulate the contact between gas diffusion layers and bipolar plate in PEMFC, and 3. electrical resistances between copper electrodes were directly measured using a Zhengyang ZY9858 digital micro-ohmmeter.

Table 2
X-ray diffraction angles of peaks and lattice constant of the four alloys.

Alloys	θ_{111} (°)	θ_{200} (°)	θ_{220} (°)	a (nm)
Hastelloy B	21.61	25.15	37.05	0.3621
Hastelloy C-276	22.02	25.54	37.39	0.3573
Monel 400	22.26	25.87	37.93	0.3532
304SS	21.80	25.26	37.25	0.3601

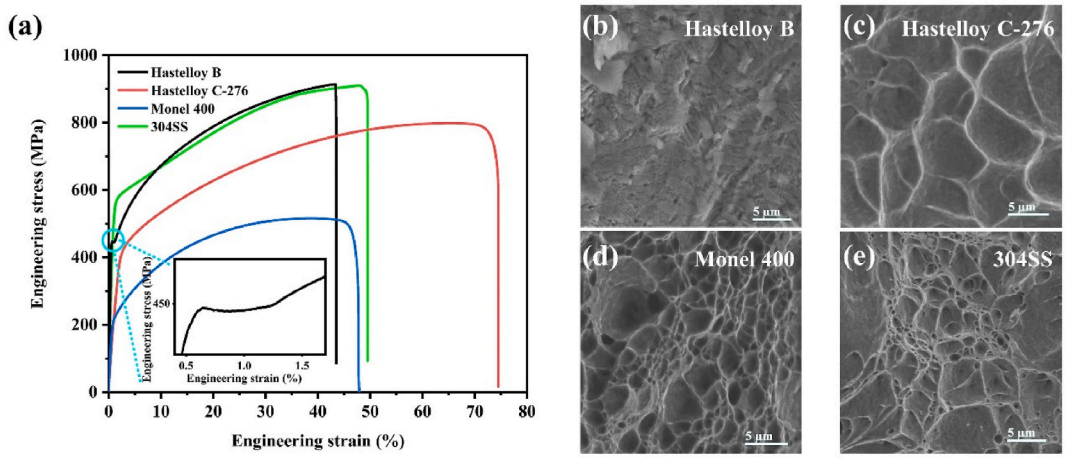

Fig. 3. (a) Tensile stress–strain curves (Inset shows the yield stage of Hastelloy B); (b)–(e) SEM images of the fracture surface of the four alloys.

Table 3
Mechanical properties of the four alloys.

Alloys	Yield strength 0.2% offset (MPa)	Ultimate tensile strength (MPa)	Uniform elongation (%)	Hardness (HV)
Hastelloy B	446.3 ± 3.8	913.6 ± 5.3	43.2 ± 1.2	311.0 ± 3.8
Hastelloy C-276	414.1 ± 5.5	797.4 ± 6.1	72.5 ± 1.5	363.7 ± 9.5
Monel 400	205.4 ± 7.5	515.3 ± 7.5	45.3 ± 1.4	167.9 ± 4.3
304SS	568.5 ± 5.6	907.5 ± 5.4	48.3 ± 1.8	219.0 ± 6.5

3. Results and discussion

3.1. Phase

The phase of four alloys was examined by XRD, and the results are shown in Fig. 2. The XRD pattern of each alloy is a typical face-centered cubic (FCC) polycrystalline diffraction pattern [19] with only three clear peaks between 2θ of 35° and 80°. No precipitates or individual elements were identified in each XRD pattern, indicating a good alloying status. According to Bragg equation $2d_{hkl}\ sin\ \theta = n\lambda$ and the crystal plane spacing formula of FCC $d_{hkl} = \frac{a}{\sqrt{h^2+k^2+l^2}}$, the lattice constant a of each alloy can be calculated by diffraction angle θ. The values are summarized in Table 2. For 304SS, its lattice constant of 0.3601 nm is almost same as the 0.3600 nm of JCPDS no. 31–0619. For Monel 400, its lattice constant of 0.3532 nm is slightly smaller than the 0.3595 nm of JCPDS no. 09–0205 (Cu3.8Ni) because of the composition difference. The XRD pattern of Hastelloy C-276 is close to the data reported by Hao et al. [20]. The XRD patterns of Hastelloy B and 304SS are all close to those in literature [21,22]. Thus, XRD demonstrates that all four alloys exhibit single-phase FCC structure.

3.2. Mechanical properties

The tensile stress–strain curves of the four alloys are shown in Fig. 3a, and their yield strength 0.2% offset, ultimate tensile strength, uniform elongation, and Vickers hardness are summarized in Table 3. All four alloys demonstrate good ductility. During the tensile test, they undergo elastic deformation, followed by plastic deformation until fracture. Only Hastelloy B exhibits a yield stage as shown in the inset of Fig. 3a. Hastelloy B and 304SS exhibit high strength. The yield strength 0.2% offset of 304SS reaches 568.5 MPa, and the ultimate tensile strength of Hastelloy B reaches 913.6 MPa. Meanwhile, Hastelloy C-276 exhibits excellent ductility with uniform elongation of 72.5%. For hardness, Hastelloy B (311.0 HV) and Hastelloy C-276 (363.7 HV) exhibit higher hardness than Monel 400 (167.9 HV) and 304SS (219.0 HV). Alloying elements such as Mo and/or W in Hastelloy alloys are dissolved in the γ matrix, which can

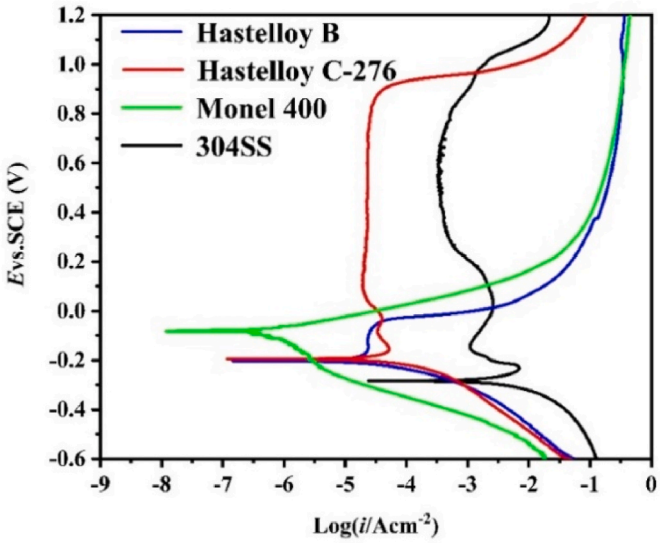

Fig. 4. Potentiodynamic polarization curves of the four alloys.

Table 4
Electrochemical properties of the four alloys.

Alloys	E_{ocp} (V)	E_{corr} (V)	I_{corr} (A·cm^{-2})	Weight loss (g)
Hastelloy B	−0.17	−0.20	$4.1 \times 10^{-4} \pm 1.3 \times 10^{-10}$	0.0853 ± 0.0010
Hastelloy C-276	−0.01	−0.19	$2.1 \times 10^{-4} \pm 2.2 \times 10^{-10}$	0.0759 ± 0.0015
Monel 400	−0.06	−0.08	$5.9 \times 10^{-7} \pm 1.2 \times 10^{-12}$	0.0718 ± 0.0013
304SS	−0.31	−0.28	$3.6 \times 10^{-3} \pm 2.9 \times 10^{-8}$	0.0875 ± 0.0020

significantly increase the hardness of Hastelloy alloy [12].

The fracture surface of the four alloys were observed using SEM to analyze the fracture mechanism. The fracture surface of Hastelloy B (Fig. 3b) exhibits many steps that intersect each other and form a river pattern, indicating a certain cleavage fracture [23], and has the lowest uniform elongation of 43.2%. This phenomenon occurs because Hastelloy B has a high Mo content (20.1 wt%) that can largely increase the brittleness of the alloy [24]. The fracture surfaces of Hastelloy C-276, Monel 400, and 304SS exhibit large number of dimples and a continuous fiber network as shown in Fig. 3c–e, which are typical ductile fracture surfaces indicating the good ductility of these three alloys. This finding is in agreement with their uniform elongation data of 72.5%, 45.3%, and 48.3% for Hastelloy C-276, Monel 400, and 304SS, respectively. In particular, the dimple size of Hastelloy C-276 is larger than those of Monel 400 and 304SS, indicating that Hastelloy C-276 has a larger plastic deformation before fracture. This feature is in agreement with its highest elongation.

The main function of bipolar plates in PEMFC is to support the electrode material, collect and conduct current, segregate oxidants and reducing agents, and guide the flow of oxidants and reducing agents on the inner surface of the electrode [8]. Therefore, good mechanical properties such as sufficient strength and ductility are highly desired. By contrast, the tensile strength and hardness of graphite are only 12.4–17.2 MPa [25] and 0.4 HV [26], respectively. Such poor mechanical properties of graphite bipolar plate inevitably cause poor durability [17]. Thus, metal bipolar plates such as Ni-based alloys and stainless steel have the advantages of admirable mechanical properties over graphite bipolar plates.

3.3. Corrosion resistance

Each alloy was subjected to electrochemical test in a simulated PEMFC electrolyte to evaluate the corrosion resistance of four alloys in the acidic work environments of PEMFC. The potentiodynamic polarization curves of four alloys are shown in Fig. 4. The open circuit potential (E_{ocp}), corrosion potential (E_{corr}), corrosion current density (I_{corr}), and weight loss after electrochemical properties test are summarized in Table 4. The results showed that the three Ni-based alloys have better corrosion resistance than 304SS. In particular, Monel 400 exhibits a relatively positive E_{corr} of −0.08V and a small I_{corr} of 5.9×10^{-7} A cm^{-2}, indicating that it is the only alloy whose corrosion current density meets the 2025 DOE target (<1 μA cm^{-2}) [17].

The surface morphologies of the four alloys before and after electrochemical properties test were observed using SEM as shown in Fig. 5. All four alloys present a machined surface with a filamentous texture before electrochemical property test (Fig. 5a–d). After the test, intergranular corrosion and pitting corrosion occur in Hastelloy B and Hastelloy C-276 (Fig. 5e and f). Hastelloy B is more corrosive than Hastelloy C-276 because that the grain boundaries of Hastelloy C-276 are more susceptible to corrosion due to the smaller

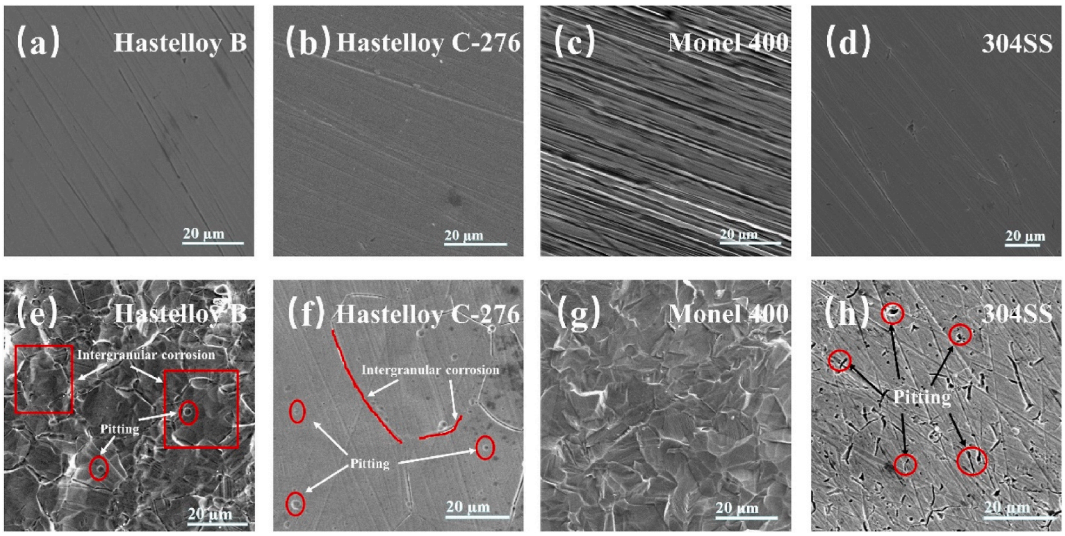

Fig. 5. SEM images of the surface of the four alloys (a)–(d) before and (e)–(h) after electrochemical property test.

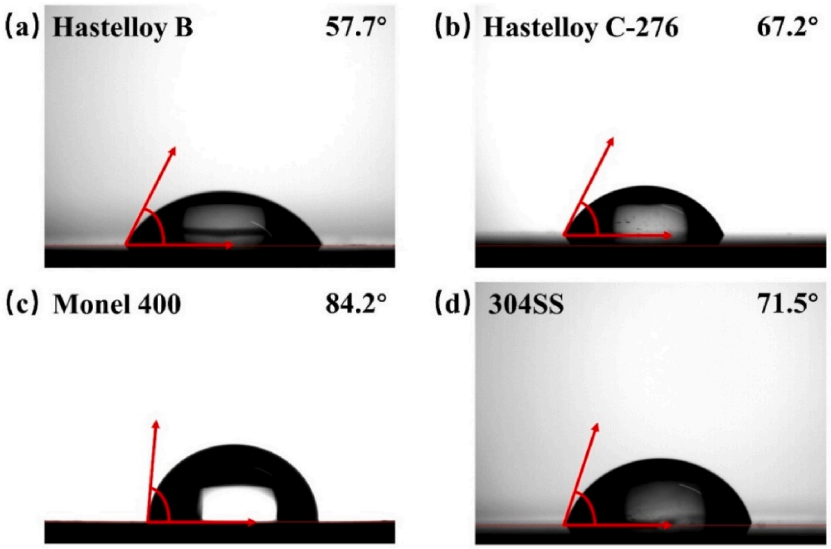

Fig. 6. Water contact angle of (a) Hastelloy B, (b) Hastelloy C-276, (c) Monel 400, (d) 304SS

concentration of Mo at grain boundaries [27]. However, Monel 400 exhibits good stability during electrochemical properties test without localized corrosion, such as intergranular corrosion or pitting corrosion (Fig. 5g), which is similar to the corrosion behavior of Monel 400 in 40% HF acid at 50 °C [28]. This phenomenon occurs because Ni compounds are not as stable as Cu compounds [29]. Therefore, Monel 400 shows better corrosion resistance than Hastelloy C-276 in the environment of HF acid. 304SS mainly exhibits pitting corrosion as shown in Fig. 5h. The passivation film of 304SS is mainly based on Cr elements, and that of Cr ions is formed due to the selective dissolution of Fe ions, allowing Cr to be enriched in the passivation film [30]. Thus, the electrochemical property test indicates that Hastelloy B, Hastelloy C-276, and 304SS suffer from serious corrosion in the simulated acidic work environment of PEMFC, and Monel 400 can withstand such harsh work environment.

3.4. Hydrophobicity

For bipolar plates, water management is important in improving PEMFC performance [31] to avoid the accumulation of water in the cathode, thus preventing the deterioration of mass transfer and the occurrence of corrosion [32]. The hydrophobicity of the four alloys was evaluated by WCA, and the measurement results are shown in Fig. 6. The WCAs of Hastelloy B (Fig. 6a), Hastelloy C-276 (Figs. 6b), and 304SS (Fig. 6d) are all smaller than 75°, indicating their poor hydrophobicity that is in agreement with previous reports

Table 5
Surface roughness of the four alloys.

Alloys	Rq (μm)
Hastelloy B	0.07 ± 0.01
Hastelloy C-276	0.18 ± 0.03
Monel 400	0.27 ± 0.04
304SS	0.24 ± 0.05

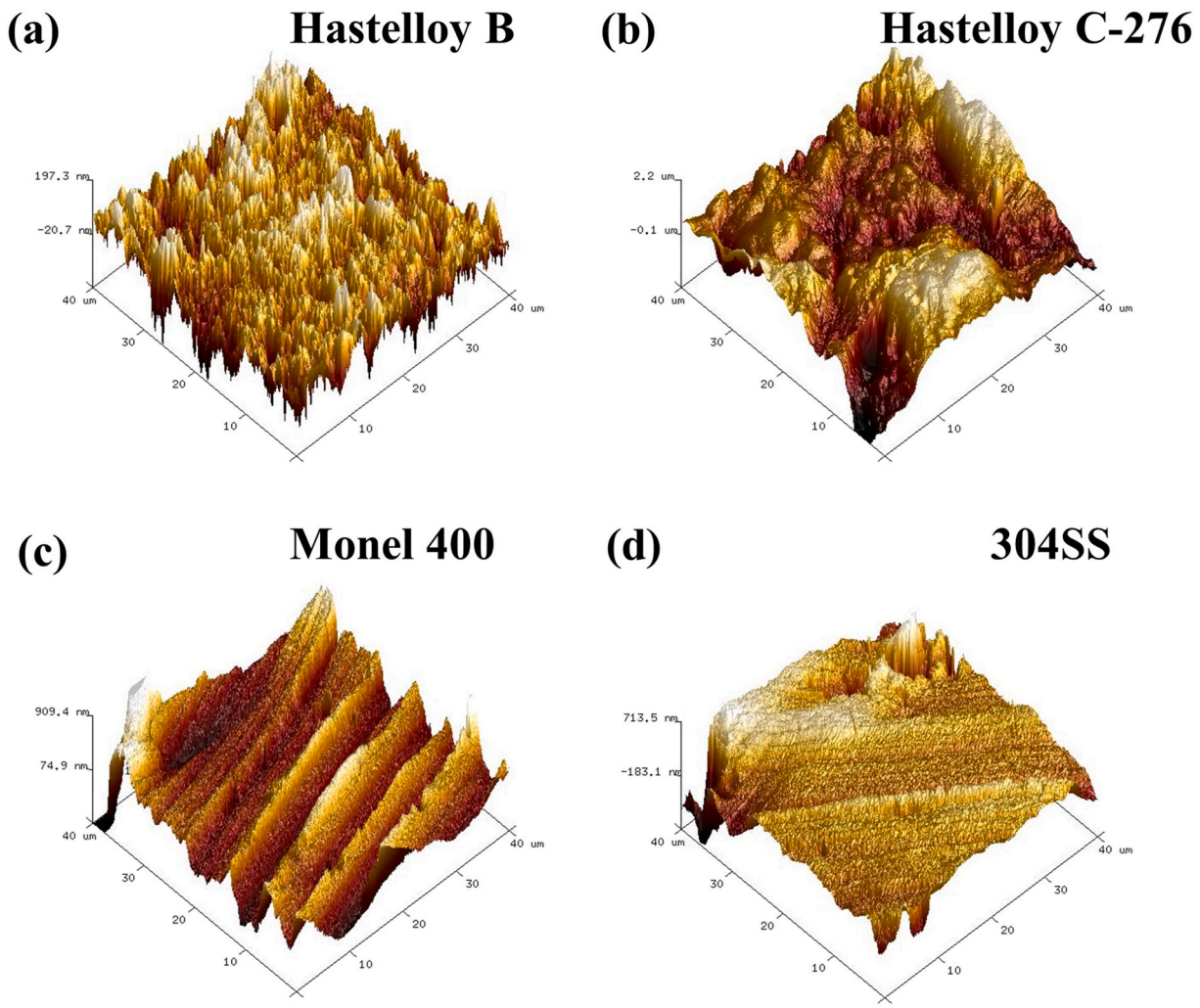

Fig. 7. AFM images of the surface of (a) Hastelloy B, (b) Hastelloy C-276, (c) Monel 400, (d) 304SS

[33,34]. However, the WCA of Monel 400 can reach 84.2° (Fig. 6c), indicating that it has the best hydrophobicity among the four alloys. The hydrophobicity of a material is related to its surface roughness and passivation layer. The rougher the surface, the more hydrophobic the surface [35]. Root mean square roughness (Rq) (Table 5) obtained from the AFM morphologies of Hastelloy B (Fig. 7a), Hastelloy C-276 (Fig. 7b), Monel 400 (Figs. 7c) and 304SS (Fig. 7d) demonstrate that Monel 400 has the highest roughness. Although its WCA is still smaller than 90°, Monel 400 can reach a close hydrophobicity state.

3.5. ICR

The conductivity of bipolar plates is a key factor in the efficiency of PMEFCs [36]. ICR can lead to a reduction in the power density of PEMFCs. Therefore, reducing the ICR is a key issue for PEMFC. Fig. 8 shows the ICR measurements for the four alloys at different levels of compaction force. The ICR of each alloy decreases extremely rapidly with the increasing compaction force and gradually remains stable at high compaction force. This phenomenon is due to the gradual increase in the effective contact area under high load

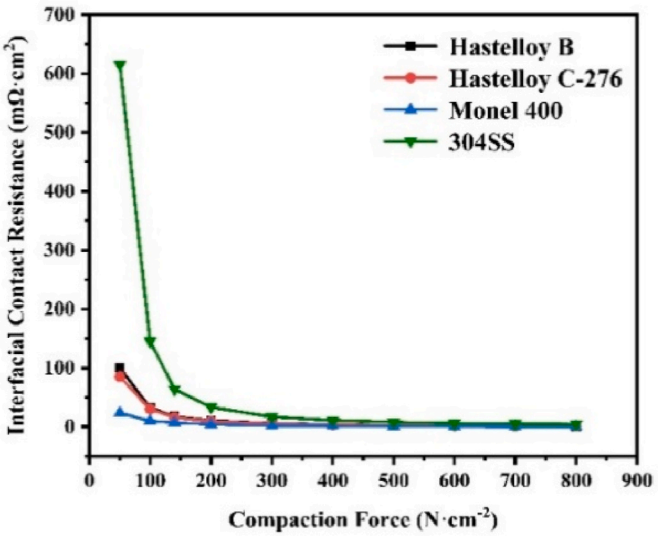

Fig. 8. ICR of the four alloys at different levels of compaction force.

Table 6
ICR of the four alloys at 140 N/cm.^{2}.

Alloys	ICR (mΩ·cm^2)
Hastelloy B	17.8 ± 3.1
Hastelloy C-276	16.3 ± 2.3
Monel 400	7.2 ± 1.3
304SS	64.2 ± 5.1

conditions, causing the resistance to decrease rapidly. When the contact area gradually becomes constant, the ICR remains basically stable under high compaction force. Table 6 shows the ICR of the four alloys recorded at a compaction force of 140 N/cm^2 [37]. The ICR of 304SS (64.2 mΩ cm^2) is larger than those of other three alloys. The ICR of 304SS is in agreement with previously reported data [38]. Therefore, stainless steel is not a good conductor because of the high Cr ion surface passivation layer [39]. By contrast, Monel 400 demonstrates good conductivity and reaches an ICR of 7.2 mΩ cm^2 at 140 N/cm^2, which meets the 2025 DOE target (<10 mΩ cm^2) [17]. The surface passivation layer of Monel 400 contains high amounts of Cu ions, which can largely increase the conductivity of Monel 400 [18].

4. Conclusions

The physical and electrochemical properties of three typical Ni-based corrosion resistance alloys and 304 stainless steel are comprehensively studied for PEMFC bipolar plate applications. All four alloys have good mechanical properties because they all exhibit single-phase FCC structure. However, the corrosion resistances and ICRs of four alloys have significant difference. Hastelloy B, Hastelloy C-276, and 304SS have low corrosion resistances and high ICRs when subjected to a simulated acidic work environment of PEMFC. Hence, they cannot meet the 2025 DOE target. Fortunately, Monel 400 exhibits a high corrosion resistance in the simulated acidic work environment of PEMFC with a corrosion current density of 5.9×10^{-7} A cm^{-2} and a low ICR of 7.2 mΩ cm^2 at 140 N cm^{-2}, thus meeting the 2025 DOE targets. Therefore, Monel 400 demonstrates excellent corrosion resistance and conductivity and is a good candidate for PEMFC metal bipolar plate of uncoated alloy materials.

Author contribution statement

Jiacheng Zhong: Conceived and designed the experiments; Performed the experiments; Analyzed and interpreted the data; Wrote the paper.

Beirui Hou, Wenmin Zhang: Performed the experiments; Analyzed and interpreted the data.

Zhansheng Guo: Analyzed and interpreted the data.

Chunwang Zhao: Conceived and designed the experiments; Analyzed and interpreted the data; Contributed reagents, materials, analysis tools or data; Wrote the paper.

Data availability statement

Data included in article/supp. material/referenced in article.

Declaration of competing interest

The authors declare the following financial interests/personal relationships which may be considered as potential competing interests: Chunwang Zhao reports financial support was provided by the National Natural Science Foundation of China.

Acknowledgments

This work was supported by the National Natural Science Foundation of China (No. 11972221), the Guangdong Key Laboratory for Hydrogen Energy Technologies (No.2018B030322005), the Innovation Team of Universities of Guangdong Province (No. 2020KCXTD011) and the Engineering Research Center of Universities of Guangdong Province (No. 2019GCZX002).

References

[1] Y.C. Lyu, Y.C. Liu, Z.E. Yu, N. Su, Y. Liu, W.X. Li, Q. Li, B.K. Guo, B. Liu, Recent advances in high energy-density cathode materials for sodium-ion batteries, Sustain. Mater. Techn. 21 (2019), e00098-e00119.
[2] Y. Leng, P.W. Ming, D.J. Yang, C.M. Zhang, Stainless steel bipolar plates for proton exchange membrane fuel cells: materials, flow channel design and forming processes, J. Power Sources 451 (2020) 227783–227806.
[3] K. Jiao, J. Xuan, Q. Du, Z.M. Bao, B. Xie, B.W. Wang, Y. Zhao, L.H. Fan, H.Z. Wang, Z.J. Hou, Designing the next generation of proton-exchange membrane fuel cells, Nature 595 (2021) 361–369.
[4] V. Rajaei, H. Rashtchi, K. Raeissi, M. Shamanian, The study of Ni-based nano-crystalline and amorphous alloy coatings on AISI 304 stainless steel for PEM fuel cell bipolar plate application, Int. J. Hydrogen Energy 42 (2017) 14264–14278.
[5] P. Mandal, U. kumar Chanda, S. Roy, A review of corrosion resistance method on stainless steel bipolar plate, Mater. Today: Proc. 5 (2018) 17852–17856.
[6] M.H. Chen, J.C. Ding, S.H. Kwon, Q.M. Wang, S.H. Zhang, Corrosion resistance and conductivity of NbN-coated 316L stainless steel bipolar plates for proton exchange membrane fuel cells, Corrosion Sci. 196 (2022) 110042–110052.
[7] A.P. Manso, F.F. Marzo, X. Garicano, C. Alegre, A. Lozano, F. Barreras, Corrosion behavior of tantalum coatings on AISI 316L stainless steel substrate for bipolar plates of PEM fuel cells, Int. J. Hydrogen Energy 45 (2020) 20679–20691.
[8] K. Xiong, W. Wu, S. Wang, L. Zhang, Modeling, design, materials and fabrication of bipolar plates for proton exchange membrane fuel cell: a review, Appl. Energy 301 (2021) 117443–117466.
[9] F.Y. Yan, B.L. Jiang, B.J. Liu, C. Yang, D. Dong, J. Shi, Retention mechanism and conductivity corrosion resistance performance of Ag doped GLC and TiN films for metal bipolar plates, Vacuum (2022) 111702–111715.
[10] B.T. Lin, C.Y. Yang, T.C. Li, X.R. Wang, C.C. Kuo, Application of ANFIS to predict springback in U-bending of nickel-based alloy, Int. J. Adv. Des. Manuf. Technol. 120 (2022) 6435–6461.
[11] Y.H. Li, S.Z. Wang, J.Q. Yang, D.H. Xu, Y. Guo, L.L. Qian, W.H. Song, Corrosion characteristics of a nickel-base alloy C-276 in harsh environments, Int. J. Hydrogen Energy 42 (2017) 19829–19835.
[12] T. Zhao, S. Zhang, Z.Y. Wang, C.H. Zhang, D.X. Zhang, N.W. Wang, C.L. Wu, Cavitation erosion/corrosion synergy and wear behaviors of nickel-based alloy coatings on 304 stainless steel prepared by cold metal transfer, Wear 510 (2022) 204510–204529.
[13] I.M. Razumovskii, A.V. Ruban, V.I. Razumovskiy, A.V. Logunov, V.N. Larionov, O.G. Ospennikova, V.A. Poklad, B. Johansson, New generation of Ni-based superalloys designed on the basis of first-principles calculations, Mater. Sci. Eng. 497 (2008) 18–24.
[14] S.S. Sawant, B.D. Gajbhiye, S. Tyagi, C.S. Sona, R. Divya, C.S. Mathpati, A. Borgohain, N.K. Maheshwari, High temperature corrosion studies in molten salt using salt purification and alloy coating, Indian Chem. Eng. 59 (2017) 242–257.
[15] Y.H. Zhu, H. Liu, J.Z. Wang, F.Y. Yan, Antagonistic effect of electrochemical corrosion on the mechanical wear of Monel 400 alloy in seawater, Corrosion Sci. 198 (2022) 110120–110132.
[16] A.R. Kannan, S.M. Kumar, R. Pramod, N.S. Shanmugam, M. Vishnukumar, S.G. Channabasavanna, Microstructure and corrosion resistance of Ni-Cu alloy fabricated through wire arc additive manufacturing, Mater. Lett. 308 (2022) 131262–131266.
[17] Y.X. Song, C.Z. Zhang, C.Y. Ling, M. Han, R.Y. Yong, D.E. Sun, J.R. Chen, Review on current research of materials, fabrication and application for bipolar plate in proton exchange membrane fuel cell, Int. J. Hydrogen Energy 45 (2020) 29832–29847.
[18] M.M. Ghorbani, R. Taherian, M. Bozorg, Investigation on physical and electrochemical properties of TiN-coated Monel alloy used for bipolar plates of proton exchange membrane fuel cell, Mater. Chem. Phys. 238 (2019) 121916–121923.
[19] T. Sakamoto, K. Asazawa, J. Sanabria-Chinchilla, U. Martinez, B. Halevi, P. Atanassov, P. Strasser, H. Tanaka, Combinatorial discovery of Ni-based binary and ternary catalysts for hydrazine electrooxidation for use in anion exchange membrane fuel cells, J. Power Sources 247 (2014) 605–611.
[20] S.P. Hao, Y. Wang, H.L. Suo, Q. Jia, M. Liu, L. Ma, Continuous electropolishing technique for long-length Hastelloy C-276 tape, Rare Met. 37 (2018) 795–802.
[21] B. Liu, X.L. Wei, W.L. Wang, J.F. Lu, J.J. Ding, Corrosion behavior of Ni-based alloys in molten NaCl-CaCl2-MgCl2 eutectic salt for concentrating solar power, Sol. Energy Mater. Sol. Cell. 170 (2017) 77–86.
[22] Y.H. Chung, T.C. Chen, H.B. Lee, L.W. Tsay, Effect of micro-shot Peening on the fatigue performance of AISI 304 stainless steel, Metals 11 (2021) 1408–1420.
[23] A. Pineau, A.A. Benzerga, T. Pardoen, Failure of metals I: brittle and ductile fracture, Acta Mater. 107 (2016) 424–483.
[24] L.C. Olson, J.W. Ambrosek, K. Sridharan, M.H. Anderson, T.R. Allen, Materials corrosion in molten LiF–NaF–KF salt, J. Fluor. Chem. 130 (2009) 67–73.
[25] G.S. Brady, H.R. Clauser, J.A. Vaccari, Materials Handbook, fifteenth ed., McGraw-Hill, 2002.
[26] D.R. Lide, CRC Handbook of Chemistry and Physics, 90th Edition, CRC Press/Taylor and Francis, 2010.
[27] K.S. Bal, J.D. Majumdar, A.R. Choudhury, Study of intergranular corrosion mechanism of fiber laser welded 3-mm-thick Hastelloy C-276 sheet, Corrosion Sci. 157 (2019) 406–419.
[28] H.L. Dai, S.W. Shi, L. Yang, J.Q. Hu, C.M. Liu, C. Guo, X. Chen, Effects of elemental composition and microstructure inhomogeneity on the corrosion behavior of nickel-based alloys in hydrofluoric acid solution, Corrosion Sci. 176 (2020) 108917–108927.
[29] Y.P. Li, X.D. Xu, Y.H. Hou, C. Zhang, F.L. Wang, K. Omura, Y. Koizumi, A. Chiba, Regulating the passive film of NiCoCrMo alloy in hydrofluoric acid solution by small addition of Cu, Corrosion Sci. 98 (2015) 119–127.
[30] J.Y. Wang, W.H. Li, H.L. Yang, H. Huang, S.X. Ji, J.M. Ruan, Z.L. Liu, Corrosion behavior of CoCrNi medium-entropy alloy compared with 304 stainless steel in H2SO4 and NaOH solutions, Corrosion Sci. 177 (2020) 108973–108984.
[31] Z.D. Wang, B. Zhang, K.X. Gao, R.X. Liu, Adjustable TiN coatings deposited with HiPIMS on titanium bipolar plates for PEMFC, Int. J. Hydrogen Energy 47 (2022) 39215–39224.
[32] C.H. Lin, S.Y. Tsai, An investigation of coated aluminium bipolar plates for PEMFC, Appl. Energy 100 (2012) 87–92.

[33] M.G. Wu, C.D. Lu, D.P. Tan, T. Hong, G.H. Chen, D.H. Wen, Effects of metal buffer layer for amorphous carbon film of 304 stainless steel bipolar plate, Thin Solid Films 616 (2016) 507–514.
[34] B.S. Yilbas, H. Ali, Laser texturing of Hastelloy C276 alloy surface for improved hydrophobicity and friction coefficient, Opt Laser. Eng. 78 (2016) 140–147.
[35] L.X. Zhang, N.M. Lin, J.J. Zou, X.Z. Lin, Z.Q. Liu, S. Yuan, Y. Yu, Z.X. Wang, Q.F. Zeng, W.G. Chen, Super-hydrophobicity and corrosion resistance of laser surface textured AISI 304 stainless steel decorated with Hexadecyltrimethoxysilane (HDTMS), Opt Laser. Technol. 127 (2020) 106146–106156.
[36] M. Atapour, V. Rajaei, S. Trasatti, M.P. Casaletto, G.L. Chiarello, Thin niobium and niobium nitride PVD coatings on AISI 304 stainless steel as bipolar plates for PEMFCs, Coatings 10 (2020) 889–906.
[37] P.C. Zhang, C.M. Hao, Y.T. Han, F.M. Du, H.Y. Wang, X.Y. Wang, J.C. Sun, Electrochemical behavior and surface conductivity of NbC modified Ti bipolar plate for proton exchange membrane fuel cell, Surf. Coating. Technol. 397 (2020) 126064–126071.
[38] H.Y. Shen, L. Wang, J.C. Sun, Characteristics and properties of Cr N compound layer produced by plasma nitriding of Cr-electroplated of AISI 304 stainless steel, Surf. Coating. Technol. 385 (2020) 125450–125458.
[39] D.P. Davies, P.L. Adcock, M. Turpin, S.J. Rowen, Bipolar plate materials for solid polymer fuel cells, J. Appl. Electrochem. 30 (2000) 101–105.